

## NUMERICAL ANALYSIS OF THE AIR-DISPLACEMENT OF VISCOPLASTIC LIQUIDS IN CAPILLARY TUBES

**Mônica F. Naccache**

Pontifícia Universidade Católica do Rio de Janeiro, Rio de Janeiro - RJ 22453-900, Brazil  
naccache@mec.puc-rio.br

**Paulo R. de Souza Mendes**

Pontifícia Universidade Católica do Rio de Janeiro, Rio de Janeiro - RJ 22453-900, Brazil  
pmendes@mec.puc-rio.br

**Abstract.** A numerical study of the displacement of viscoplastic fluids in capillary tubes by air is performed. This situation is encountered in many applications such as flow through porous media in enhanced oil recovery and coating flows. In these processes it is important to understand the mechanism of liquid displacement and to determine the amount of liquid left behind adjacent to the wall. The non-Newtonian fluid behavior alters the flow kinematics and changes the amount of mass left at the tube wall as compared to the Newtonian case. The numerical solution is obtained by solving the conservation equations of mass and momentum, via the finite volume method, and using the volume of fluid method to model the multiphase flow. In order to model the viscoplastic behavior of the liquid, the Generalized Newtonian Liquid constitutive equation was employed, in conjunction with a recently proposed viscosity function (de Souza Mendes and Dutra, 2004). Two rheological parameters appear in the dimensionless form of this equation, both of them obtained experimentally via least squares data fit. One parameter is the power-law index and the other one is the jump number, which gives the size of the shear rate jump that occurs as the stress reaches the yield stress while the viscosity undergoes a sharp decrease. The numerical results are obtained for unsteady inertialess flow. Velocity and stress fields, as well as the interface shape and the amount of mass left attached to the wall, are obtained for different combinations of flow and rheological parameters. It was observed that the thickness of the film of liquid left on the wall increases asymptotically with the flow rate and with the power-law index. Also, it is shown that it slightly decreases with the jump number.

**keywords:** Viscoplastic fluid, air-displacement

### 1. Introduction

In this work, the displacement of a viscoplastic liquid by air inside a tube is analyzed numerically. This situation is found in several industrial applications, such as coating flows and flow through porous media. In these processes, it is important to determine the amount of liquid that remains adjacent to the wall. Fairbrother and Stubbs, 1935 and Taylor, 1961 determined experimentally the mass fraction deposited on the tube wall for a Newtonian inertialess flow. The mass deposited on the tube wall  $m$  is given by:

$$m = \frac{U - \bar{u}}{U} = 1 - \left( \frac{R_b}{R} \right)^2 \quad (1)$$

where  $U$  is the velocity of the tip of the interface,  $\bar{u}$  is the mean velocity of the viscoplastic liquid far ahead the air-liquid interface,  $R$  is the tube radius and  $R_b$  is the bubble radius, as it is shown in Fig. 1. The results obtained by Taylor, 1961 were later expanded by Cox, 1962, and show that the mass deposited on the tube wall increases with the Capillary number ( $Ca \equiv \mu U / \sigma$ , where  $\mu$  is the viscosity and  $\sigma$  is the surface tension) until an asymptotic value of 0.60, when the capillary number reaches a value of 10.

Lee *et al.*, 2002 and Quintella *et al.*, 2005 analyzed numerically the displacement of viscoelastic fluids by air, using the finite element method. The first ones analyzed the flow between parallel plates, while Quintella *et al.*, 2005 analyzed the flow in capillaries. Giavedoni and Saita, 1997 performed a literature review concerning the theoretical modelling of gas-liquid displacement between parallel plates. Goldsmith and Mason, 1963, Teletzke *et al.*, 1988, Bretherton, 1961 and Soares *et al.*, 2005 studied the liquid-liquid displacement inside tubes. The results obtained by Soares *et al.*, 2005 show the effects of different parameters on the interface shape and on the mass deposited on the wall.

In this work, a numerical analysis of the displacement of a viscoplastic liquid by air inside a tube, is performed. All the results were obtained for low Reynolds numbers and negligible surface tension. The effects of rheological and flow parameters on the mass deposited at wall, and on the flow pattern were obtained and discussed.

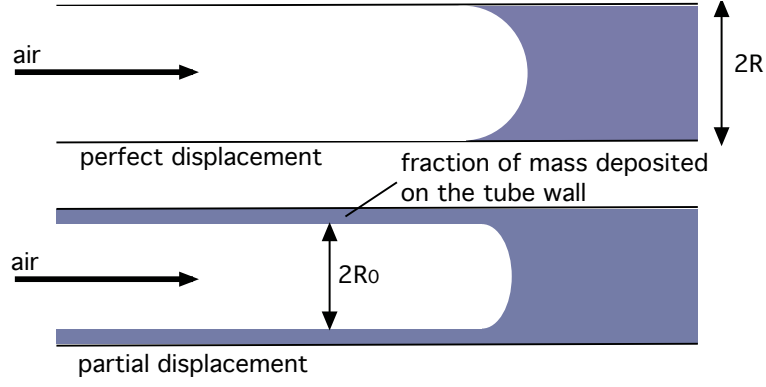


Figure 1: The geometry

## 2. Mathematical modeling

The flow under study is shown in Fig. (1). The multiphase flow was modeled by the volume of fluid method (VOF), that solves a set of mass conservation equations and obtains the volume fraction of each phase  $\alpha_i$  through the domain, which should sum up unity inside each control volume. Therefore, if:

- $\alpha_i = 0$  - the volume does not contain the phase  $i$ ;
- $\alpha_i = 1$  - the volume contains only the phase  $i$ ;
- $0 < \alpha_i < 1$  - the volume contains the interface.

In this study, only two phases are present. Both fluids, air and the non-Newtonian liquid, are assumed incompressible. The multiphase flow was solved obtaining the solution of the conservation equations for a transient and laminar flow regime. The properties appearing in the transport equations  $\phi$ , are given by:

$$\phi = \alpha_2 \phi_2 + (1 - \alpha_2) \phi_1 \quad (2)$$

The interface between phases is obtained by the solution of continuity equation for the volume fraction  $\alpha_1$ :

$$\frac{\partial \alpha_1}{\partial t} + \text{div}(\alpha_1 \mathbf{v}) = 0 \quad (3)$$

where  $\mathbf{v}$  is the velocity vector. The volume fraction equation for the secondary phase 2 is obtained from the following constraint equation:

$$\alpha_1 + \alpha_2 = 1 \quad (4)$$

The momentum conservation equations for the mixture are:

$$\frac{\partial(\rho \mathbf{v})}{\partial t} + \text{div}(\rho \mathbf{v} \mathbf{v}) = -\text{grad } p + \text{div}[\eta(\text{grad} \mathbf{v} + \text{grad} \mathbf{v}^T)] + \rho \mathbf{g} \quad (5)$$

where  $\rho$  is the density,  $p$  is the pressure,  $\mathbf{g}$  are the components of the gravity acceleration vector and  $\eta = (\alpha_1 \eta_1 + \alpha_2 \eta_2)$  is the viscosity of the mixture. In the problem analyzed,  $\eta_2$  is the air viscosity and  $\eta_1$  is the viscosity of the viscoplastic fluid, given by the model proposed by Souza Mendes and Dutra (2004), the SMD equation:

$$\eta = (1 - \exp(-\eta_0 \dot{\gamma} / \tau_0)) \left( \frac{\tau_0}{\dot{\gamma}} + K \dot{\gamma}^{n-1} \right) \quad (6)$$

In this equation, four rheological parameters appear: the plateau of constant viscosity for lower strain rates  $\eta_0$ , the yield stress  $\tau_0$ , the behavior index  $n$ , and the consistency index  $K$ . It is worth mentioning that in this equation, when the stress reaches the yield stress, there is a sharp increase of shear rate with a constant stress. The shear rate jumps from  $\dot{\gamma}_0 \equiv \tau_0 / \eta_0$  to a much larger value  $\dot{\gamma}_1 \equiv (\tau_0 / K)^{1/n}$ .

## 2.1. Dimensionless analysis

The governing dimensionless parameters were obtained choosing  $\dot{\gamma}_1$  as the characteristic shear rate and  $\tau_0$  as the characteristic shear stress. Therefore,  $\dot{\gamma}^* = \dot{\gamma}/\dot{\gamma}_1$  and  $\tau^* = \tau/\tau_0$ . It is also interesting to define a new rheological dimensionless parameter, the Jump number  $J$ , which gives a measure of the shear jump that occurs when  $\tau = \tau_0$ . Then,

$$J \equiv \frac{\dot{\gamma}_1 - \dot{\gamma}_0}{\dot{\gamma}_0} = \frac{\eta_0 \tau_0^{\frac{1-n}{n}}}{K^{1/n}} \quad (7)$$

Therefore, the dimensionless viscosity function,  $\eta^* = \tau^*/\dot{\gamma}^*$ , is given by:

$$\eta = (1 - \exp[-(J+1)\dot{\gamma}^*]) \left( \frac{1}{\dot{\gamma}^*} + \dot{\gamma}^{*n-1} \right) \quad (8)$$

It is worth mentioning that when  $J \rightarrow \infty$  the SMD equation approaches the Herschel-Bulckley model Bird *et al.*, 1987. The dimensionless conservation equations are given by:

$$\frac{\partial \alpha_1}{\partial t^*} + \text{div}(\alpha_1 \mathbf{v}^*) = 0 \quad (9)$$

$$\frac{\partial \mathbf{v}^*}{\partial t^*} + \text{div}(\mathbf{v}^* \mathbf{v}^*) = -\text{grad} P^* + \frac{1}{Re} \text{div} [\eta^* (\text{grad} \mathbf{v}^* + \text{grad} \mathbf{v}^{*T})] \quad (10)$$

In the above equations, the dimensionless variables are defined as following:

$$t^* = t\dot{\gamma}_1 \quad x^* = \frac{x}{R} \quad r^* = \frac{r}{R} \quad \mathbf{v}^* = \frac{\mathbf{v}}{\dot{\gamma}_1 R} \quad (11)$$

The dimensionless modified pressure is given by:

$$P^* = \frac{p}{\rho(\dot{\gamma}_1 R)^2} - \frac{gr^* \sin \theta}{\dot{\gamma}_1^2 R} \quad (12)$$

The Reynolds number is defined as

$$Re = \frac{\rho \dot{\gamma}_1 R^2}{\eta_c} \quad (13)$$

where  $\eta_c$  is the characteristic viscosity, calculated at the characteristic shear rate,  $\dot{\gamma}_1$ . Another important dimensionless parameter is the Capillary number, which is here defined as

$$Ca_p = \frac{\tau_0 R}{\sigma} \quad (14)$$

where  $\sigma$  is the surface tension.

## 3. Numerical solution

The numerical solution of the governing equations was obtained using the Fluent software. The finite volume method (Patankar, 1980) was used to obtain the conservation equations discretization, using a second-order upwind scheme for the momentum equation and a first-order upwind scheme for the volume fraction equation. The unsteady terms were discretized using an implicit fomulation. Staggered velocity components were employed to avoid unrealistic pressure fields and the PISO algorithm (Fluent-User's-Guide, 2006) was used, in order to couple the pressure and velocity. The boundary conditions were the no slip condition at tube wall, symmetry at tube center, constant inlet velocity and fully developed flow condition at outlet boundary. As the initial condition it was assumed that the tube was completely full of the viscoplastic liquid, and at the entrance the volume fraction of air was set equal to unity.

A non-uniform mesh was used in the numerical simulation, with 202 control volumes in the axial direction, and 40 control volumes in the radial direction. Some mesh tests were performed to validate the numerical solution and the mesh used. The Newtonian results were compared to the results obtained by Taylor, 1961. The error obtained for the mass deposited at the tube wall ( $e = |m_{num} - m_{Taylor}|/m_{Taylor}$ ) was equal to 2%. The results for non-Newtonian cases were compared to results obtained with more refined meshes. The difference in the mass deposited at the tube wall, between the mesh used and a  $302 \times 60$  mesh, was equal to 3%. Another important parameter in the numerical solution is the time step. Some instabilities were observed for higher values of time steps. In the results obtained in this work, the time steps used varied from  $10^{-4}$  to  $10^{-5}$  s. However, it is worth mentioning that the value of mass deposited has shown to be very sensitive to the numerical solution parameters. In some cases, a reliable solution could only be achieved with very low time steps and very strong convergence criterium, leading to extremely large CPU times.

All the numerical results were obtained for negligible surface tension, or  $Ca_p \rightarrow \infty$ . Convergence problems were observed for finite capillary numbers.

#### 4. Results and discussion

All the numerical solutions were obtained for a ratio of tube diameter and tube length equal to 20, since the flow pattern had become invariant before this point. The effects of some governing parameters, on flow pattern and on the amount of mass deposited at wall, were investigated. All the results were obtained for low Reynolds numbers and infinite Capillary numbers. Its worth mentioning that the dimensionless mean entrance velocity ( $u^*$ ) and the dimensionless developed wall shear stress ( $\tau_w^*$ ) are equivalent parameters. The effects of these parameters and of the rheological parameters  $J$  and  $n$  were investigated, and are presented below. The values for the rheological parameters used in the simulations were chosen based on real rheological data for a Carbopol aqueous solution.

##### 4.1. Flow pattern results

The flow pattern can be analyzed with the aid of Figs. (2)-(8), which show some results of the dimensionless velocity, strain rate, and shear stress fields. Only the region of the domain that contains the bubble front is shown. The black line appearing in these figures indicates the interface between the fluids, as it is marked in Fig. (2). The interface line was defined as the line where  $\alpha_1 = \alpha_2 = 0.5$ . Figure (2) shows the velocity magnitude field for  $J = 1.5 \times 10^6$  and  $n = 0.41$ ,

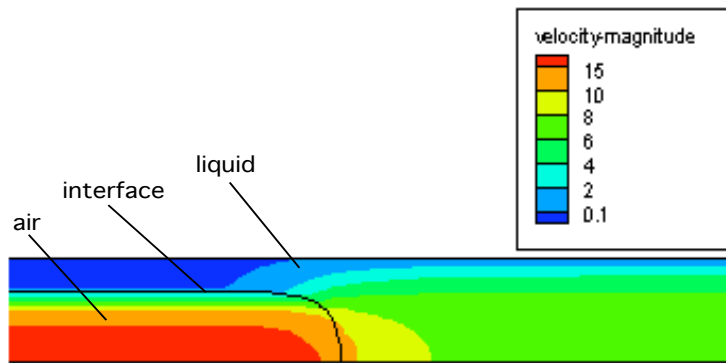


Figure 2: Velocity magnitude for  $u^* = 5$ ,  $\tau_w^* = 5.1$ ,  $J = 1.5 \times 10^6$  and  $n = 0.41$

and  $u^* = 5$ . It shows negligible velocity values in a region between the interface and the tube wall, which defines the mass deposited region. Also, it can be observed that the highest velocities occur inside the bubble, as expected. Figures (3)- (8) show the strain rate and shear stress for  $J = 1.5 \times 10^6$  and  $n = 0.41$ , for three different dimensionless inlet velocities,  $u^* = 1, 5$  and  $10$ . These cases correspond to a dimensionless shear stress at wall, far away the bubble front, equal to  $\tau_w^* = 3.2, 5.1$  and  $6.4$ , respectively.

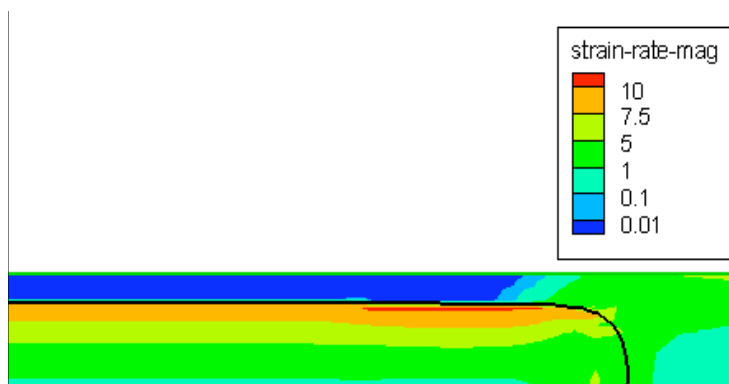


Figure 3: Strain rate field for  $u^* = 1$ ,  $\tau_w^* = 3.2$ ,  $J = 1.5 \times 10^6$  and  $n = 0.41$

It can be observed that the thickness of the film of liquid left on the wall increases as the flow rate is increased. For each flow rate, it can be noted that the deposited liquid mass, behind the bubble front is shear-stress free, as expected. Ahead of the bubble front, the wall shear stress becomes constant and equal to the the fully-developed flow value. Also, in this region a plug flow zone appears near the centerline, with low strain rates values. For low flow rates the region of

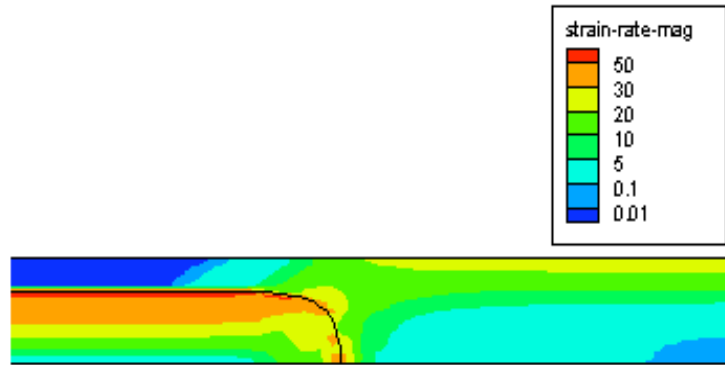


Figure 4: Strain rate field for  $u^* = 5$ ,  $\tau_w^* = 5.1$ ,  $J = 1.5 \times 10^6$  and  $n = 0.41$

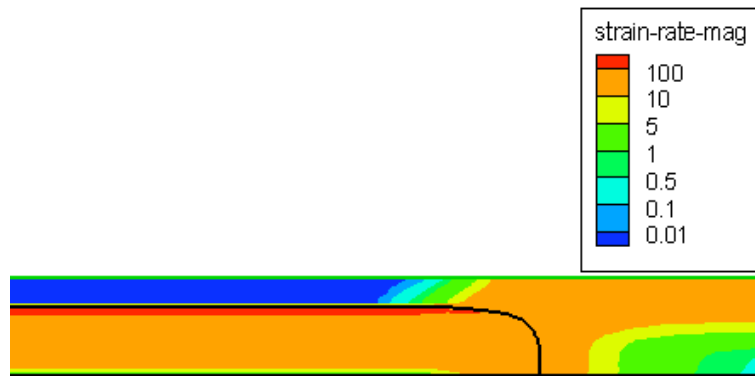


Figure 5: Strain rate field for  $u^* = 10$ ,  $\tau_w^* = 6.4$ ,  $J = 1.5 \times 10^6$  and  $n = 0.41$

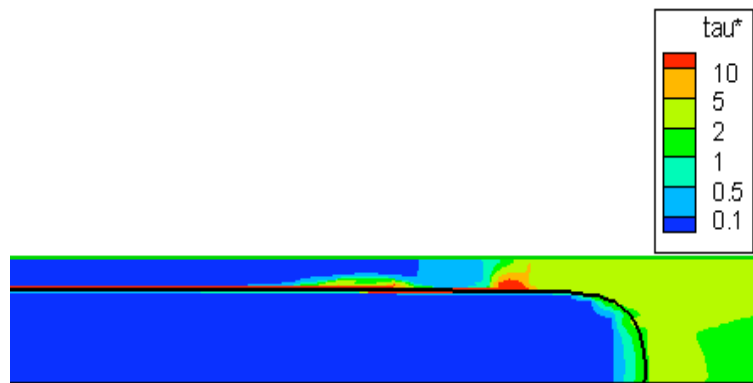


Figure 6: Stress field for  $u^* = 1$ ,  $\tau_w^* = 3.2$ ,  $J = 1.5 \times 10^6$  and  $n = 0.41$

influence of the bubble front on shear rate and shear stress is rather short. However, this region increases as the flow rate is increased. Therefore, fully developed flow occurs at shorter distances from the bubble front for lower flow rates.

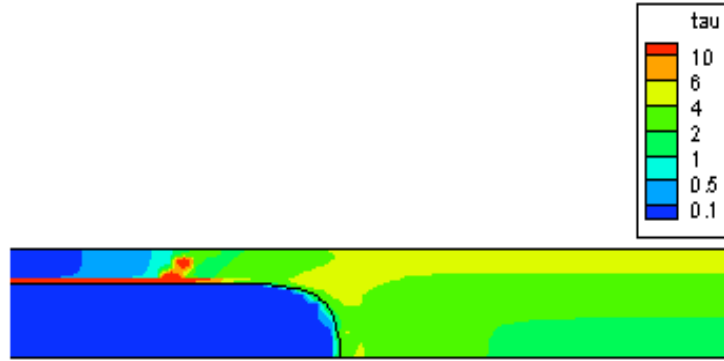


Figure 7: Stress field for  $u^* = 5$ ,  $\tau_w^* = 5.1$ ,  $J = 1.5 \times 10^6$  and  $n = 0.41$

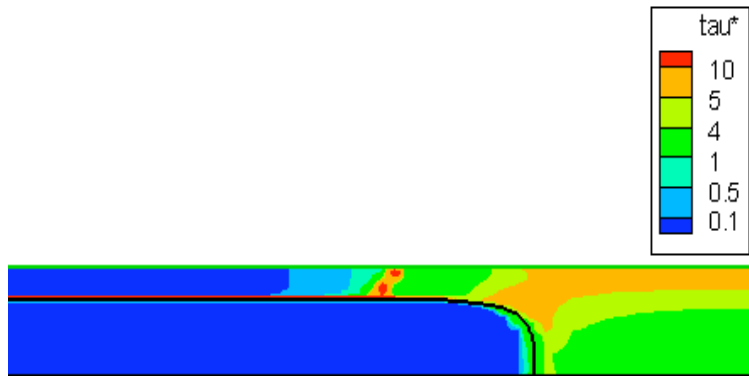


Figure 8: Stress field for  $u^* = 10$ ,  $\tau_w^* = 6.4$ ,  $J = 1.5 \times 10^6$  and  $n = 0.41$

Figures (9) and (10) show the strain rate and stress field for  $J = 1.5 \times 10^6$  and  $n = 1$ ,  $u^* = 5$  and  $\tau_w^* = 21.3$ . Comparing this result with the ones show in Figs. (4) and (7), it can be observed that an increase in the behavior index  $n$  leads to an increase of the curvature of the bubble front, and of the mass deposited. It can be observed that the strain rates are of the same order of magnitude of the case with  $n = 0.41$ . However, as  $n$  is increased, the viscosities are higher, which leads to higher stresses. The region of influence of the bubble front on shear rate and shear stress also seems to increase with  $n$ .

The influence of the Jump number on flow pattern can be evaluated comparing the results shown in Figs. (11) and (12), with the ones show in Figs. (4) and (4). Figures (11) and (12) showed the strain rate and stress field for  $J = 1.5 \times 10^3$ ,  $n = 0.41$ ,  $u^* = 1$  and  $\tau_w^* = 3.2$ , while Figs. (4) and (4) show the result for a higher Jump number,  $J = 1.5 \times 10^6$ . It can be observed that Jump number almost does not affect the stress and strain rate fields. Also, the bubble shape and influence of the bubble front seem to be unaffected by the Jump number. This result was expected, since the viscosity is only affected by the Jump number in regions of lower strain rates, which only occur at the mass deposited region.

#### 4.2. Amount of mass deposited results

The effects of rheological parameters and of the flow rate on the amount of mass deposited in the tube wall can be analyzed with the aid of Figs. (13)-(15). Figure (13) shows the influence of the flow rate on the mass deposited on tube wall. It can be observed that the mass deposited increases as flow rate is increased, until an asymptotic value. This asymptotic value is lower than the Newtonian limit for infinite capillary numbers, which is equal to 0.6. Therefore, viscoplasticity decreases the amount of mass deposited at the tube wall. The effect of Jump number is shown in Fig. (14). Is can be noted that the Jump number slightly decreases the amount of mass deposited at wall. This result also shows that the efficiency of the liquid displacement process is increased by viscoplasticity. Finally, the effect of the behavior index can be analyzed with the aid of Fig. (15). The mass deposited increases with  $n$  until an asymptotic value, that is equal to

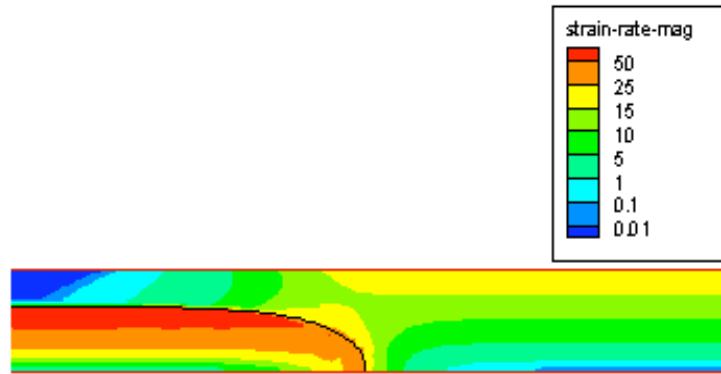


Figure 9: Strain rate field for  $u^* = 5$ ,  $\tau_w^* = 21.3$ ,  $J = 1.5 \times 10^6$  and  $n = 1$

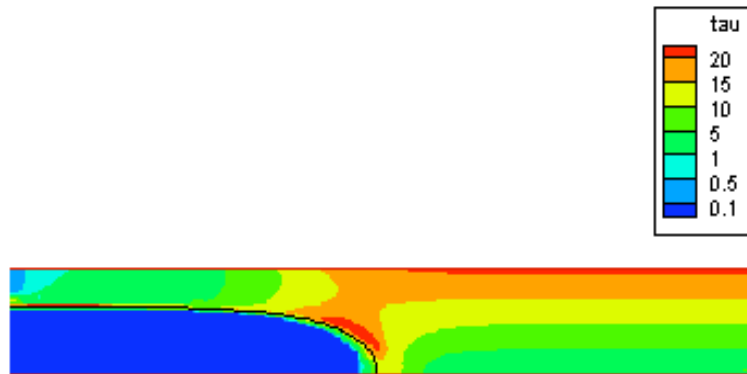


Figure 10: Stress field for  $u^* = 5$ ,  $\tau_w^* = 21.3$ ,  $J = 1.5 \times 10^6$  and  $n = 1$

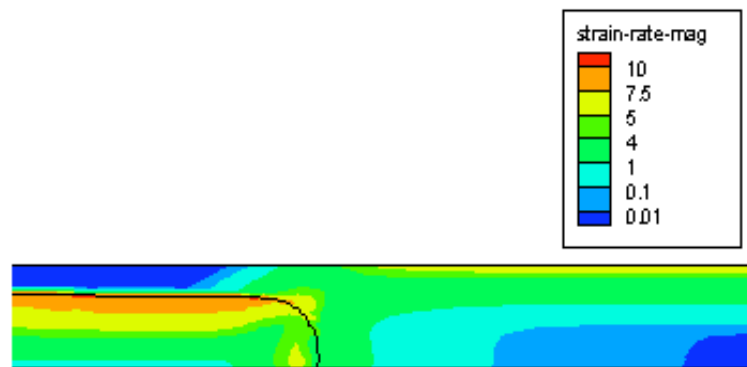


Figure 11: Strain rate field for  $u^* = 1$ ,  $\tau_w^* = 3.2$ ,  $J = 1.5 \times 10^3$  and  $n = 0.41$

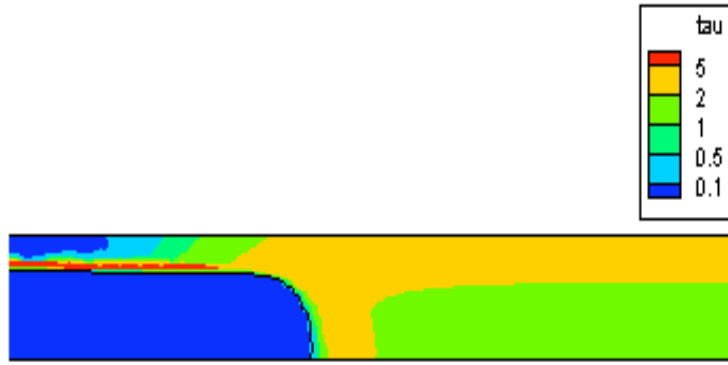


Figure 12: Stress field for  $u^* = 1$ ,  $\tau_w^* = 3.2$ ,  $J = 1.5 \times 10^3$  and  $n = 0.41$

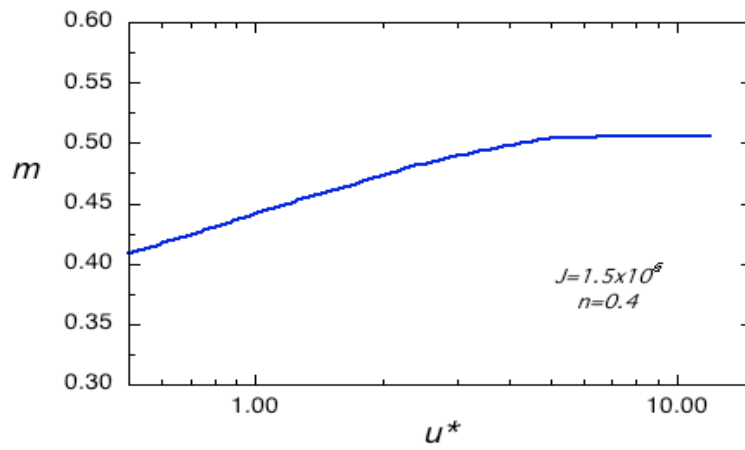


Figure 13: Mass fraction deposited at tube wall versus  $u^*$  for  $J = 1.5 \times 10^6$  and  $n = 0.41$

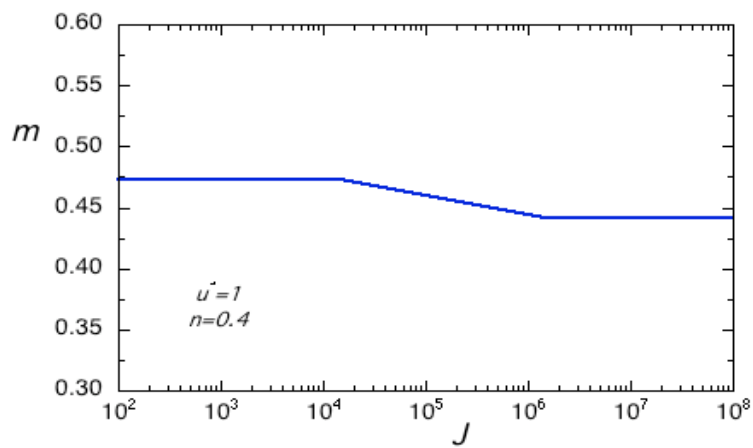


Figure 14: Mass fraction deposited at tube wall versus  $J$  for  $n = 0.41$  and  $u^* = 1$

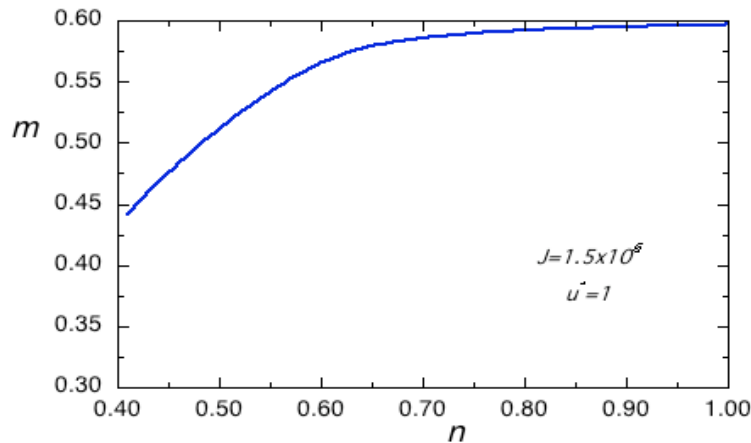


Figure 15: Mass fraction deposited at tube wall versus  $n$  for  $J = 1.5 \times 10^6$  and  $u^* = 5$

the Newtonian value. Its worth mentioning that when  $n = 1$ , the viscosity model is similar to the Bingham model with a constant viscosity plateau when the stress is below yield stress.

## 5. Final Remarks

In this work, the displacement of viscoplastic fluids by air inside tubes was analyzed numerically. The main goal was to obtain the amount of liquid left behind, adjacent to the wall, for different flow and rheological parameters. Larger amounts of liquid deposited at the tube wall mean lower displacement efficiencies. The results were obtained for unsteady and low Reynolds number flow. The governing conservation equations were discretized via the finite volume technique, using the volume of fluid method to model the multiphase flow. The viscoplastic behavior of the liquid was modeled by the Generalized Newtonian Liquid constitutive equation, using the SMD viscosity function. Velocity, strain rate and stress fields, and the amount of mass left attached to the wall, were obtained for different combinations of flow and rheological parameters. It was observed that the thickness of the film of liquid left on the wall increases with the behavior index, reaching as asymptotic value equal to the Newtonian one, as  $n$  goes to one. The amount of mass deposited also increases asymptotically as the flow rate is increased. It was also shown that the amount of mass deposited decreases as the jump number increases, but the Jump number effect is rather small.

## 6. Acknowledgements

Financial support for the present research was provided by Petrobras, CNPq and MCT - Brazil

## 7. References

- Bird, R. B., Armstrong, R. C., and Hassager, O., 1987, "Dynamics of Polymeric Liquids", Vol. I, John Wiley & Sons.
- Bretherton, F. P., 1961, The motion of long bubbles in tubes, "J. Fluid Mech.", Vol. 10, pp. 166–188.
- Cox, B. G., 1962, On driving a viscous fluid out of a tube, "J. Fluid Mech.", Vol. 14, pp. 81–96.
- de Souza Mendes, P. R. and Dutra, E. S. S., 2004, Viscosity function for yield-stress liquids, "Applied Rheology", Vol. 14, No. 6, pp. 296–302.
- Fairbrother, F. and Stubbs, A. E., 1935, Studies in electroosmosis. Part IV. The bubble-tube methods of measurement, "J. Chem. Soc.", Vol. 1, pp. 527–529.
- Fluent-User's-Guide, 2006, Vol. 6.2, Fluent Inc., New Hampshire.
- Giavedoni, M. D. and Saita, F. A., 1997, The axisymmetric and plane cases of a gas phase steadily displacing a newtonian liquid: a simultaneous solution of the governing equations, "Physics of Fluids", Vol. 9, pp. 2420–2428.
- Goldsmith, H. L. and Mason, S. G., 1963, The flow of suspensions through tubes, "J. Colloid Sci.", Vol. 18, pp. 237–261.
- Lee, A. G., Shaqfeh, E. S., and Khomami, B., 2002, A study of viscoelastic free surface flows by the finite element method: Hele-shaw and slot coating flows, "J. Non-Newtonian Fluid Mech.", Vol. 108, pp. 327–362.
- Patankar, S. V., 1980, "Numerical Heat Transfer and Fluid Flow", Hemisphere Publishing Corporation.
- Quintella, E. F., de Souza Mendes, P. R., and Carvalho, M. S., 2005, Displacement flows of dilute polymer solutions in capillaries, "J. Non-Newtonian Fluid Mech. (submitted)".
- Soares, E. J., Carvalho, M. S., and de Souza Mendes, P. R., 2005, Gas-displacement of non-newtonian liquids in capillary tubes, "Int. J. Heat Fluid Flow (in print)".

- Taylor, G. I., 1961, Deposition of a viscous fluid on the wall of a tube, "J. Fluid Mech.", Vol. 10, pp. 161–165.
- Teletzke, G. F., Davis, H. T., and Scriven, L. E., 1988, Wetting hydrodynamics, "Revue de Physique Appliquee", Vol. 23, pp. 989–1007.